Adsorption of Water on the TiO_2 (Rutile) (110) Surface: A Comparison of Periodic and Embedded Cluster Calculations

A. V. Bandura,[†] D. G. Sykes,[‡] V. Shapovalov,[#] T. N. Troung,[#] J. D. Kubicki,*[,§] and R. A. Evarestov[†]

St. Petersburg State University, St. Petersburg, Russia, Department of Chemistry and Department of Geosciences and the Materials Research Institute, The Pennsylvania State University, University Park, Pennsylvania 16802, and Henry Eyring Center for Theoretical Chemistry, Department of Chemistry, Univeristy of Utah

Received: October 16, 2003; In Final Form: March 3, 2004

Periodic density functional theory (DFT) based on plane waves (PW) and Hartree−Fock (HF) based on the linear combination of atomic orbitals (LCAO) calculations using slabs separated by vacuum gaps were carried out to model the H_2O-TiO_2 (rutile) (110) interface. Positions of all atoms were allowed to relax except atoms in the central layer of the slab. Both associative and dissociative adsorption mechanisms were considered for half-monolayer and monolayer coverages. Five different orientations of H_2O molecules on the TiO_2 surface were studied to determine the most energetically favorable water positions for the associative mechanism. Two slab thicknesses (three Ti layers and five Ti layers) were chosen to test the effect of slab depth on calculated surface structures and adsorption energies. Results indicate that associative adsorption is favorable by −8 to −20 kJ/mol/H_2O depending on the slab thickness for full-monolayer coverage. Embedded cluster HF calculations were also performed for comparison. Adsorption energies of H_2O in the embedded cluster case are much more favorable for the associative mechanism. The role of H-bond formation on the adsorption energies and structures is discussed.

1. Introduction

The adsorption of water on TiO_2 surfaces has been extensively investigated using both experimental and theoretical methods. Goniakowski and Gillan[1] published one of the earliest papers on first-principles calculations of H_2O adsorption on the TiO_2 (110) surface. Further density functional theory (DFT) studies of H_2O adsorption on TiO_2 have been conducted by Vogtenhuber et al.,[2] Casarin et al.,[3] and Stefanovich et al.,[4] as well as the first-principles molecular dynamics calculations of Lindan et al.,[5] Zhang and Lindan,[6] and Langel.[7] Nevertheless, the adsorption of H_2O on the TiO_2 (110) surface is still a matter for controversy. From experiment,[8−11] it has been proposed that H_2O adsorbs mainly associatively and dissociates at defect sites. If dissociation does occur, it is only at low coverages (<15%) that may be associated with surface defects. In contrast, most DFT calculations[1,2] with the plane wave (PW) basis predict dissociation at all coverages or an equivalent amount of dissociative and associative mechanisms.[5−7] In contrast, Hartree−Fock (HF) embedded cluster calculations[4,12] with atomic (Gaussian) basis sets predict that the associative mechanism should be favored due to overestimation of H-bonding in the dissociated configuration by DFT-PW studies.[4]

Reinhardt and Hess[13] made the first 2-D periodic all-electron HF calculations of the rutile relaxed surfaces based on the linear combination of atomic orbitals (LCAO).[14] They obtained the atomic displacements of surface atoms which did not differ significantly from the later results of DFT-PW investigations.[1,2,5−7] Further periodic LCAO studies of TiO_2 surfaces have been conducted by Harrison et al.,[15] Leconte et al.,[16] and Evarestov et al.[17] Periodic HF-LCAO or DFT-LCAO methods have not been applied previously for studies of H_2O adsorption on TiO_2. To investigate the dependence of the obtained results on the method used we performed such HF-LCAO and DFT-LCAO calculations.

Research presented in this paper seeks to test various methods with periodic and embedded cluster calculations to resolve discrepancies among the methods. High-vacuum experimental work[8,9] provides a well-defined benchmark for testing computational methodologies. Hence, vacuum adsorption of H_2O onto the TiO_2 (110) surface is used as a test case. However, the long-term goal of this research is to model the interface of TiO_2 and bulk water, so solvation forces will need to be included to predict adsorption energies and surface structures. Solvation forces are difficult to include in periodic DFT calculations because a large number of H_2O molecules must be included in layers between mineral slabs to simulate bulk water. On the other hand, the HF embedded cluster approach in the program CECILIA[12] can include H-bonding to H_2O molecules not directly bonded to the surface and long-range solvation via a dielectric continuum half-space representing bulk water. The embedded cluster approach is an obvious way to develop a force field for the Ti−O−H system representing the real TiO_2-H_2O interface,[18] so consistency between this approach and the results of periodic calculations would be a useful step toward reliable molecular dynamics simulations of the larger scale mineral−water system.

2. Computational Details

DFT-PW calculations were performed on different H_2O-TiO_2 structures to determine the most stable arrangements on the rutile

[†] St. Petersburg State University.
[‡] Department of Chemistry, The Pennsylvania State University.
[#] Department of Chemistry, University of Utah.
[§] Department of Geosciences and the Materials Research Institute, The Pennsylvania State University.

10.1021/jp037141i CCC: $27.50
Published on Web 05/07/2004

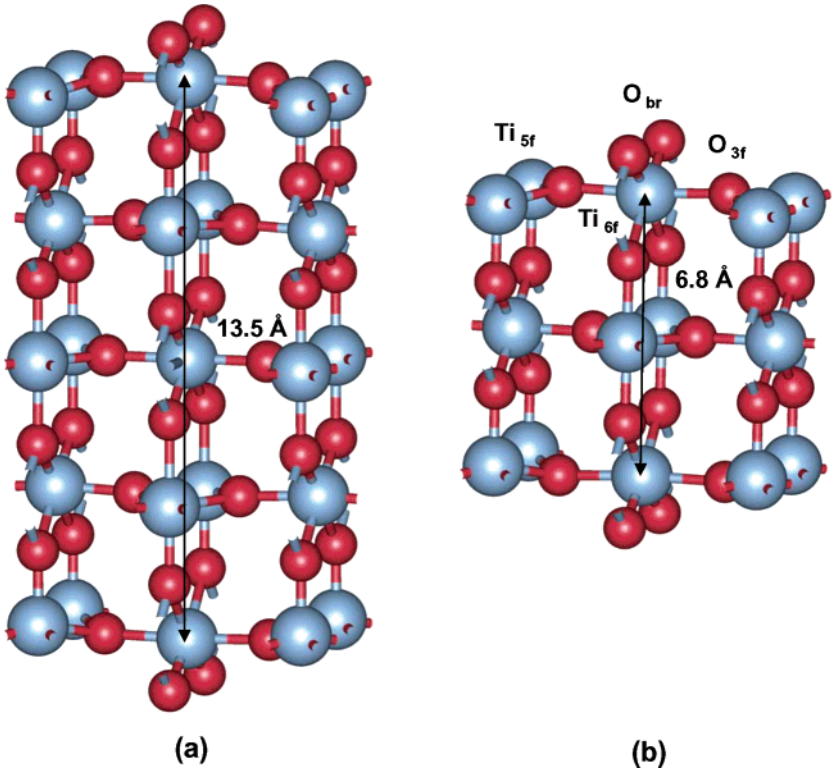

Figure 1. Comparison of the DFT-GGA-PW91-340 eV geometry optimization for five-layer (a) and three-layer (b) slabs of TiO_2. The positions of the middle-plane atoms are fixed.

(110) surface. To this end, a 3-D supercell consisting of 1×1 or 2×1 surface unit cells was used to model the (110) surface geometry (Figure 1). The (110) surface normal is in the *z*-direction with (110) faces separated by a vacuum gap. Similar structures have been studied in the other theoretical investigations.[1,5−7,13] The smallest surface unit cell was chosen for bare surface calculations, having dimensions of *c* (2.959 Å) and $\sqrt{2}a$ (6.497 Å) in the (001) and ($\bar{1}$10) directions, respectively, where *a* and *c* are translation vectors for the bulk rutile unit cell. This surface unit cell is doubled in the (001) direction for the hydroxylated or hydrated surfaces. Two types of slabs were considered: one three Ti layers thick (vacuum gap 10 Å) and the second five Ti layers thick (vacuum gap 15 Å). These two slab thicknesses were chosen to test the effect of slab depth on calculated surface structures. However, in most cases (except the structures with monolayer coverage), calculations were performed for three-layer slabs with a total cell thickness ≈19 Å (slab + vacuum gap).

Initially, two different methods of structural relaxation (models I and II) were used for the 3-D slabs. The positions of all atoms were allowed to relax for model I, but the atomic positions of the central layer were fixed at the bulk crystal geometry for model II. (Note: all 3-D calculations in this report were performed with cell parameters fixed to the experimental values.) Preliminary results obtained for models I and II did not differ significantly; hence, only the model II system was used in subsequent calculations. Model II was assumed to be more appropriate to the real 2-D surface relaxation because real crystals are not thin slabs, and the bulk crystal structure probably exists a few atomic layers beneath the mineral surface. Use of the constrained central layer was also accompanied by imposition of the inversion symmetry. This symmetry saves computational time and minimizes any possible dipole moment of the slab.

Minimum energy structures of both slab models were determined using the generalized gradient approximation (GGA) of Perdew and Wang[19] (PW91) calculations within the CASTEP[20] module of Cerius[2] (Molecular Simulations Inc., San Diego, CA). Ultrasoft pseudopotentials[21] were used in searching of the most favorable structures, allowing us to apply a small plane wave cutoff energy−340 eV. The default CASTEP Monkhorst−Pack scheme[22] was used for choosing *k*-points, and reciprocal space was sampled by special points set 2 2 1 and 3 3 1 (for the hydroxylated or hydrated slab models with a double unit cell). Test calculations using norm-conserving pseudopotentials[23] with a plane wave cutoff energy of 1000 eV and *k*-points set 3 3 1 were also conducted within CASTEP for selected structures.

The computer code CRYSTAL-2003[24] was applied for LCAO calculations. This program was designed to perform the ab initio calculations of periodic systems using Hartree−Fock or Kohn−Sham Hamiltonians via the expansion of the single particle wave functions as a linear combination of Bloch functions defined in terms of local atomic (Gaussian) orbitals.

In our HF and DFT LCAO computations, we include the same three-Ti-layer systems as were considered using the PW basis. However, the DFT method was also used for the five-Ti-layer systems. Both the associative and dissociative water monolayer adsorption has been investigated. In all cases, model II was used for TiO_2 slabs with the fixed positions of middle layer atoms. The results are discussed below in section 4 where we describe the LCAO 2-D periodic slab calculations.

The Durand−Barthelat[25] effective core pseudopotentials (ECP) and corresponding basis sets[26] for all atoms except H have been used in our LCAO calculations. This choice is due to fact that this basis set was optimized for CRYSTAL calculations of the bulk TiO_2 crystal in the rutile structure. It includes 31 G(sp) functions on O and 1-41 G(sp-d) functions on Ti. Additionally, the HF all-electron calculations have been made for three-Ti-layer slabs with extended 8-6411-41 G(s-sp-d) basis on Ti and 8-411-1 G(s-sp-d) basis on O atoms.[27] The standard 6-31G(d,p) (31-1 G(s-p)) set[28] has been used on hydrogen atoms throughout our periodic LCAO calculations.

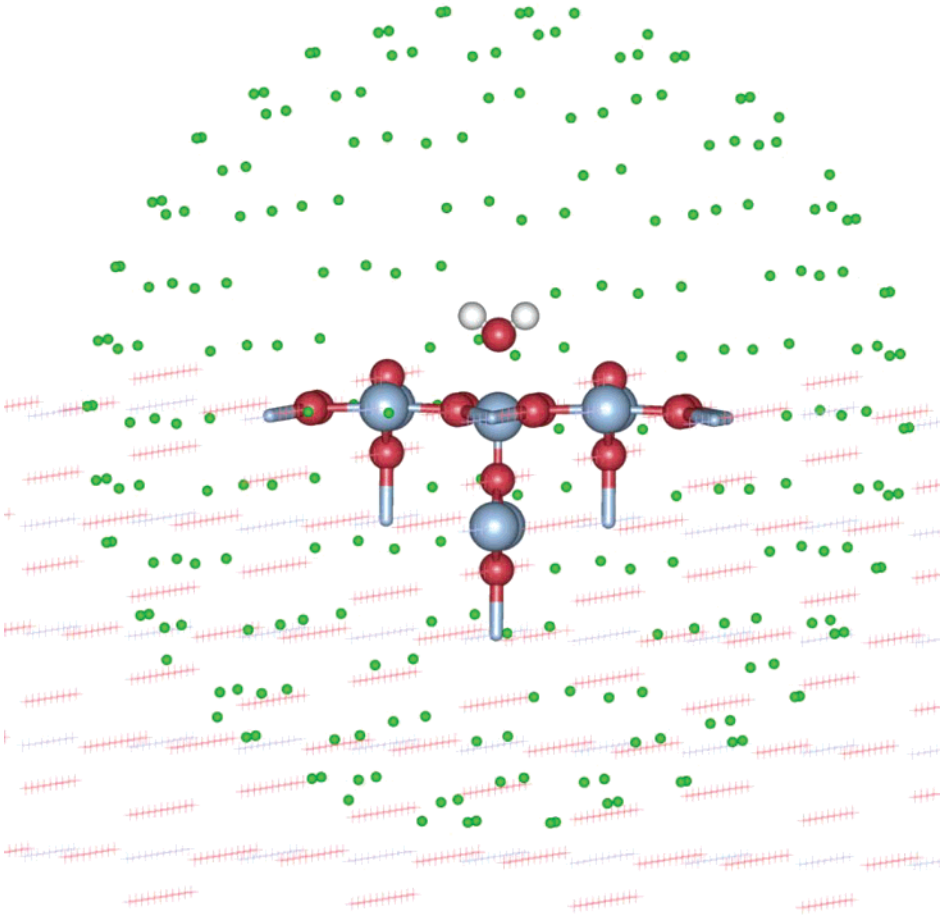

Figure 2. Embedded cluster model for Ti_7O_{14}: spheres, cluster atoms; sticks, pseudopotential cores; crosses, lattice of point-charge ions; small-sized balls, SCREEP surface point charges.

To estimate the basis set superposition error (BSSE), an HF ECP calculation was performed using the same 2 × 1 2-D cell and the same basis set for all species. Perdue−Wang (PW91)[19] exchange-correlation functionals have been used in DFT computations.

Default parameters controlling the accuracy of the integrals calculation in CRYSTAL[24] have been used for all-electron calculations. Nevertheless, in ECP computations, we have investigated the influence of the mentioned parameters on our results and found that increasing them by 2 orders of magnitude did not change the adsorption energies more than 4 kJ/mol and did not produce noticeable differences in the optimized geometry. Results reported below correspond to the increased accuracies in the integrals calculation. The reciprocal space was sampled by Monkhorst−Pack[22] special point sets 6 3 for a 1 × 1 2-D unit cell and 3 3 for a 2 × 1 2-D unit cell as it was made in the PW calculations.

Embedded cluster calculations were performed for comparison with periodic studies. The model developed by Stefanovich and Truong[12] was applied. This model utilizes a three-level interaction approach and takes into account the long-range forces properly. The central stoichiometric part of the cluster is treated by the ab initio method using pseudopotential cores of extra Ti atoms to saturate the dangling bonds of the outermost oxygen atoms. A large stoichiometric grid of point charges represents the surrounding ions, and a special array of point charges distributed on a closed surface around the cluster is constructed to reproduce the remainder of the long-range Coulomb interactions (i.e., the Madelung potential of the bulk crystal at the surface). The neutrality condition is satisfied separately for the stoichiometric part of the cluster and the lattice array of ions plus extra pseudopotential cores. In Figure 2, we show the different zones in the embedded cluster model.

Embedded cluster calculations were conducted with a modified version of Gaussian 98[29] termed CECILIA.[12] Test calculations on the Ti_7O_{14} cluster defined in ref 4 were performed to verify our results, and then calculations on larger systems of $Ti_{13}O_{26}$ (Figure 3a) and $Ti_{17}O_{34}$ (Figure 3b) were carried out. In the $Ti_7O_{14}-H_2O$ and $Ti_{13}O_{26}-H_2O$ clusters only one Ti, one bridging O, and the H_2O atoms were allowed to relax during energy minimization. In contrast, the additional four oxygen atoms (nearest to the central Ti) were free to move in the $Ti_{17}O_{34}-H_2O$ cluster. The larger cluster and greater surface relaxation were considered necessary to adequately describe the possible H-bonding arrangements of associatively and dissociatively adsorbed H_2O on the TiO_2 (110) surface. About 1000 full point charges (i.e., +4 and −2) from the four-Ti-layer slab and up to 310 partial charges fitted to the Madelung potential of the rest of crystal using the program SCREEP[12] were introduced to represent the electrostatics of the bulk TiO_2. Positions of cluster atoms and lattice ions were chosen in accordance with the experimentally determined surface relaxation.[30]

Following the work of Stefanovich and Truong,[12] we have used the LANL1 or LANL2[31] pseudopotentials for Ti atoms and the SBK[32] pseudopotential on O atoms for the HF Gaussian 98 calculations. In the case of LANL1, the 3s and 3p electrons of Ti atom are included in the atomic core, whereas in the case of LANL2 the corresponding orbitals are treated as semicore states. We used the minimum basis set[31] for Ti atoms and CEP-

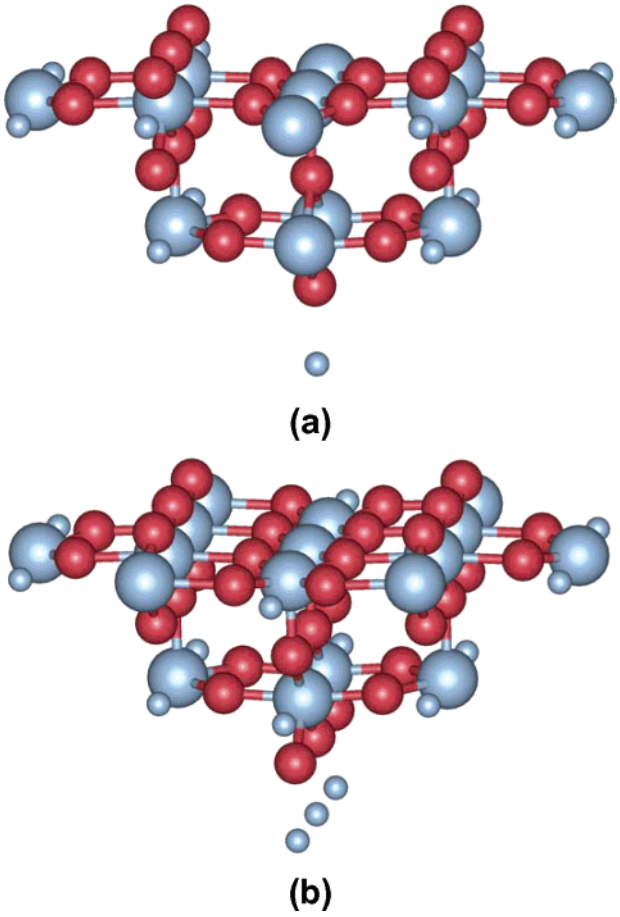

Figure 3. Central part of the embedded cluster models: $Ti_{13}O_{26}$ (a) and $Ti_{17}O_{34}$ (b). Small-sized balls represent the Ti pseudopotential cores.

31G[32] for O atoms except those in the central part of the cluster. For pseudopotential cores of Ti atoms saturating the dangling bonds only the semicore basis functions were included in the case of the LANL2 pseudopotential, whereas in the case of the LANL1 pseudopotential not all basis functions were included. This trick provides the same net charge on the extra pseudopotential Ti cores as on the lattice ions. The double-ζ basis[31] has been used on the central Ti atom in the cluster and triple-ζ CEP-121G[32] has been used on its nearest neighbor oxygens, as well as on bridging oxygens and water atoms. Polarization functions[29] have been added to all oxygens and hydrogens.

3. PW 3-D Periodic Slab Calculations

3.1. Model System Tests. Adsorption was simulated with a pair of H_2O molecules (one at each side) with the three-layer TiO_2 slab using 2×1 unit cell. The placing of one H_2O molecule on each side allows us to use a cell with inversion symmetry and creates a system with zero dipole moment associated with the slab. Generation of dipole moments within a slab can dramatically alter the results of 3-D periodic calculations,[1,33] so this methodology was adopted to minimize this problem.

Comparison of the three- and five-Ti-layer slabs of the TiO_2 (110) surfaces representing the relaxed in vacuo structures are given in Figure 1. Relaxation of surface atoms is similar for both cases. For example, compare the three Ti−O bond distances labeled in Table 1. Expansion from three to five layers changes these lengths from 2.05, 1.93, and 1.83 Å to 2.04, 1.94, and 1.82 Å, respectively (in the bulk crystal the corresponding lengths are 1.98, 1.95, and 1.95 Å). Furthermore, the overall structure does not change qualitatively between these two systems. In both relaxed structures the surface 3-fold oxygens (O_{3f}) lie almost in the same plane as 6-fold Ti (Ti_{6f}), whereas the 5-fold Ti (Ti_{5f}) is shifted down (Table 2). However, the displacement of the Ti_{5f} atom relative to the position of Ti_{6f} is different: −0.27 for the three-Ti-layer slab and −0.38 Å for the five-Ti-layer slab. The calculated *z*-shifts of the bridging oxygen (O_{br}) are considerably more positive than the experi-

TABLE 1: Ti−O Bond Lengths on the Rutile (110) Surface Obtained by DFT-PW Calculations Using the Different Energy Cutoffs and *k*-Point Sets

number of Ti layers:		3	3	3	5
energy cutoff, eV:		1000	340	340	340
Monkhorst−Pack *k*-points set:		3 3 1	3 3 1	2 2 1	2 2 1
surface model	bond	averaged length, Å			
bare, relaxed in a vacuum	$Ti_{6f}-O_{3f}$	2.04	2.05	2.05	2.04
	$Ti_{5f}-O_{3f}$	1.94	1.93	1.93	1.94
	$Ti-O_{br}-Ti$	1.87	1.83	1.83	1.82
associatively hydroxylated, monolayer	$Ti-O_{br}-Ti$	1.93	1.89	1.89	1.87
	$Ti_{5f}-O_{H_2O}$	2.22	2.27	2.25	2.30
dissociatively hydroxylated, monolayer	$Ti-O_{br}(H)-Ti$	2.02	2.02	2.02	2.02
	$Ti-O_{ter}(H)$	1.94	1.90	1.90	1.90

TABLE 2: *z*-Shifts of Ti and O Atoms on the Surface of (110) Rutile Three-Ti-Layer Models Obtained by DFT-PW Calculations Using the 3 3 1 Monkhorst−Pack *k*-Points Set

surface model:		bare, relaxed in a vacuum			associatively hydroxylated, monolayer		dissociatively hydroxylated, monolayer	
energy cutoff, eV:		1000	340	exptl[30]	1000	340	1000	340
atom type	symbol	*z*-shifts, Å						
6-fold coordinated surface Ti	Ti_{6f}	0.21	0.18	0.12 ± 0.05	0.15	0.11	0.11	0.10
5-fold coordinated surface Ti, or 6-fold coordinated terminal Ti with OH group	Ti_{5f}, or Ti_{ter}	−0.06	−0.09	−0.16 ± 0.05	−0.01	−0.06	0.04	0.01
bridging surface oxygen	O_{br}	0.08	−0.01	−0.27 ± 0.08	0.10	0.00	0.15	0.10
3-fold coordinated surface oxygens	$O_{3f,1}$	0.26	0.24	0.05 ± 0.05	0.14	0.11	0.11	0.07
	$O_{3f,2}$	0.26	0.24	−0.16 ± 0.08	0.12	0.09	0.02	0.05
oxygen underneath O_{br}	O_{uO}	0.01	−0.01	0.05 ± 0.08	0.03	0.00	0.04	0.04
oxygen underneath Ti_{5f} in the middle Ti layer	O_{uTi}	0.04	0.02	0.00 ± 0.08	0.03	0.01	0.04	0.01

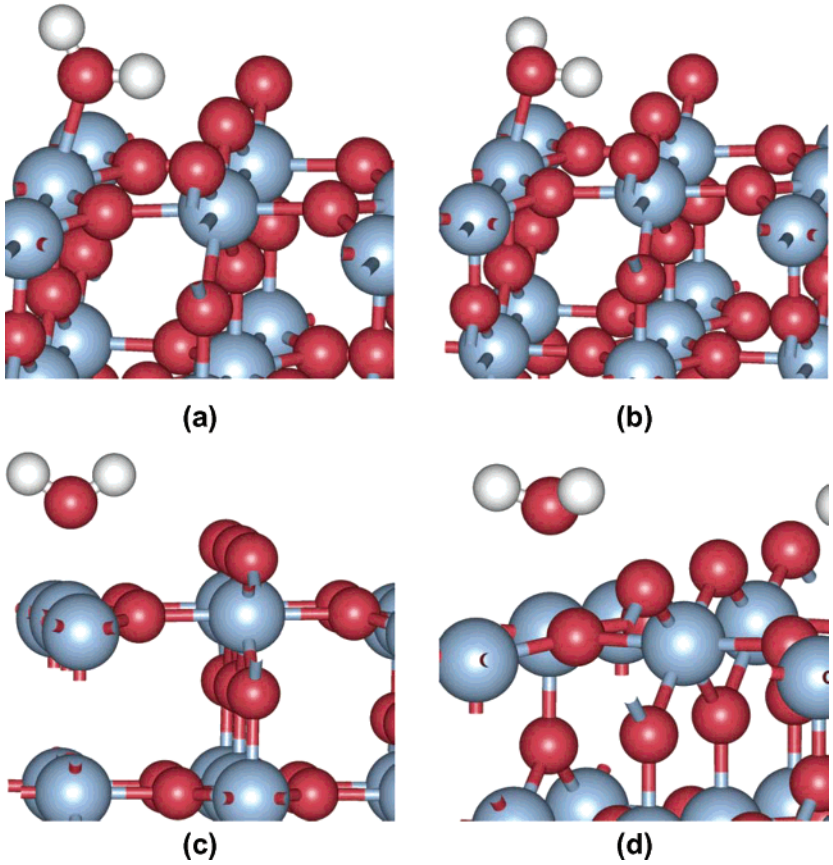

Figure 4. Associative adsorption at half-monolayer coverage: (a) structure 1; (b) structure 2; (c) structure 3; (d) structure 4.

mental values[30] (Table 2). The same disagreement was found in other DFT-PW and ab initio molecular dynamics calculations.[5] It should be noted that the calculated absolute *z*-shift depends on the number of Ti layers in the slab due to the contributions of the deep layers relaxation. The relative displacement of the O_{br} atom measured from the position of Ti_{6f} is closer to the corresponding experimental value.

3.2. Associative Water Adsorption. A half-monolayer of associatively adsorbed water was modeled first. Five different positions of the water molecule on the TiO_2 relaxed surface were considered. In all these structures, the water O was directly bonded to the five-coordinate Ti atom. Structures 1 and 2 (Figure 4) corresponded to a single H-bond between an H in H_2O and a bridging oxygen atom (O_{br}) on the TiO_2 (110) surface. All atoms of the H_2O molecule and the O_{br} were in the same plane in structure 1 (i.e., the torsion angle $H-O-H\cdots O_{br}$ is 180°), whereas this angle is 117° for structure 2. The positions of atoms of both slabs were optimized as described above, and adsorption energies have been obtained (Table 3). In each case, the CASTEP optimization procedure resulted in structures that corresponded to the local energy minima nearest to the initial geometry. The optimum structure 2 configuration had a calculated binding energy 8 kJ/mol greater than that of structure 1.

In an attempt to verify if the lowest potential energy minimum on the potential surface was reached in structure 2 (within the given model constraints), three additional configurations were investigated (Figure 4). In structure 3, the H_2O molecule had a symmetrical orientation with the O atoms on the surface, and the C_{2v} axis of the water molecule coincides with the $Ti-O(H_2)$ direction. The optimum energy of this structure was 21 kJ/mol less than the energy of structure 2 (Table 3). Further energy minimization of structure 3 proved to be possible if the C_{2v} axis of the water molecule was rotated 60° in the $(\bar{1}10)$ direction such that the H atoms of H_2O come closer to surface. This configuration (structure 4) was lower in energy than that of structure 3 but higher than that of structures 1 and 2. Structure 5 was used to investigate the possibility of forming two H-bonds between H_2O and bridging oxygens by rotating the H_2O molecule around the (110) direction (i.e., the *z*-axis) by 90°. The binding energy found for this structure was less favorable than that of the other structures (Table 3).

TABLE 3: Adsorption Energies Per Water Molecule (Without Zero-Point Correction) for Different Configurations of the H_2O Layer on the TiO_2 (110) Surface (kJ/mol)[a]

	half-monolayer coverage		monolayer coverage			
	3-Ti-layer slab		3-Ti-layer slab		5-Ti-layer slab	
structure[b]	assoc	dissoc	assoc	dissoc	assoc	dissoc
1	−90	−111				
2	−97	−113	−104	−96	−92	−77
3	−77					
4	−82					
5	−74					

[a] The values obtained in DFT-PW calculations. [b] See text for explanation.

Structure 2 (Figure 4) was thus the most favorable structure for associative adsorption of a single H_2O molecule per surface unit cell of all those modeled here. Hence, the same initial water orientation was employed to calculate the energy of a monolayer of adsorbed H_2O (i.e., two H_2O molecules per slab side). The corresponding energy is given in Table 3. Note that the adsorption energy in this case was stronger than that for half-monolayer coverage. This was due to the strong H-bond interaction between neighboring H_2O molecules that was favorable in the structure 2 orientation. Optimized atomic

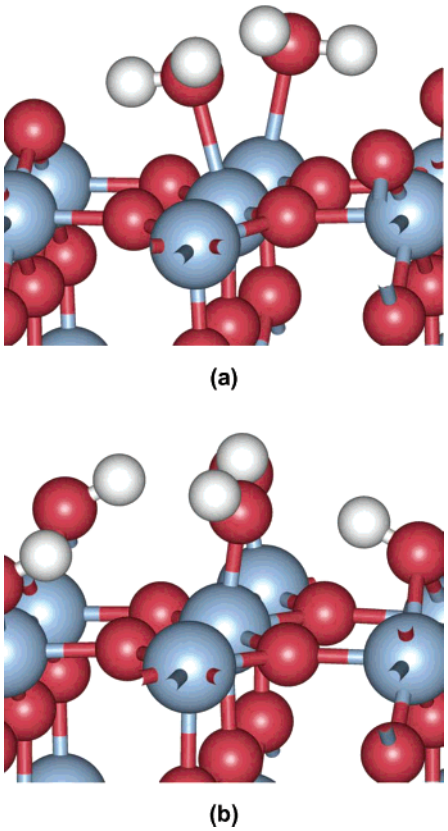

Figure 5. Structure of the water monolayer on a five-Ti-layer slab: (a) associative adsorption; (b) dissociative adsorption.

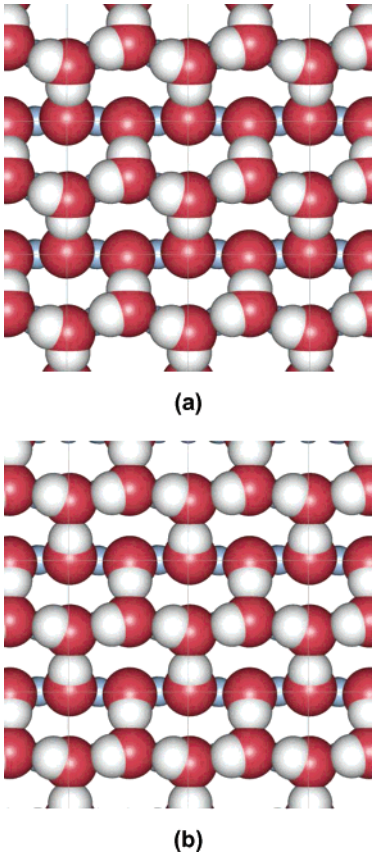

Figure 6. Oxygen−hydrogen arrangement in the water monolayer on a five-Ti-layer slab (for simplicity, only the positions of the Ti atoms of the slab are shown): (a) associative adsorption; (b) dissociative adsorption.

coordinates were then transferred to the five-Ti-layer slab as the initial configuration and a new energy minimum for this slab was reached using the CASTEP optimization procedure. The resulting structures are shown in Figures 5 and 6. Qualitatively, the relaxation of the surface atoms for monolayer coverage is the same as for relaxed in vacuo slabs, but the lowering of the Ti_{5f} atom position relative to the level of the Ti_{6f} atoms is less than that for the bare surface: −0.16 and −0.22 Å for the three- and five-Ti-layer slabs, correspondingly (Table 2). The calculated adsorption energy for the five-Ti-layer slab proved to be weaker by 12 kJ/mol than the energy for the three-Ti-layer slab (Table 3), which may be due to some excess flexibility attributed to the three-Ti-layer slab.

3.3. Dissociative Water Adsorption. The dissociative adsorption of H_2O onto the (110) surface was modeled assuming that one H atom was bonded to the O_{br} next to the Ti atom with the terminal OH group. (Note that this Ti atom was originally five-coordinate on the bare (110) surface.) Due to the half-monolayer configuration, the neighboring OH groups can be adsorbed either in a zigzag geometry or in-line. In the latter case, there exists the possibility of H-bonding between neighboring bridging and terminal OH groups: $O_{br}-H\cdots O_{ter}H$ (Figure 7). Consequently, the in-line configuration only was considered because this H-bonding should lower the adsorption energy.[5,6] As in the case of molecular H_2O adsorption, there are two possible OH orientations: in-plane, with torsion angle $H-O\cdots H-O$ equal to 180° (structure 1) and a conformation with a smaller torsion angle (structure 2.) Energy minimizations of the corresponding slabs led to similar adsorption energies (Table 3), which were lower than the corresponding associative values for half-monolayer coverage by ≈12−20 kJ/mol. Thus, our result is in accordance with previous DFT simulations[1,4,5] for half-monolayer coverage that predict H_2O dissociation on the rutile (110) surface.

A different conclusion was obtained by our calculations on models corresponding to full-monolayer coverages (Figures 5 and 6). The distinct feature of these structures, in contrast to other cases, is the nearly equivalent displacements of the Ti and O atoms on the surface Ti layer such that they lie in one plane (Table 2). Note that the overall arrangement of H and O atoms in the (110) surface is similar in both associative and dissociative adsorption (Figure 6). As has been noticed in ref 6, in some senses the dissociatively adsorbed water molecule has a highly stretched, rather than completely broken bond. However, the obtained binding energies are stronger for associative adsorption on both the three- and five-Ti-layer slabs (Table 3). This large of a difference (15 kJ/H_2O molecule) in favor of associative adsorption was not obtained in previous DFT calculations (Table 4).

3.4. Comparison to Norm-Conserving Pseudopotential Results. Norm-conserving pseudopotentials and a 1000 eV energy cutoff were used to verify the data obtained with ultrasoft pseudopotentials. Also, we investigated the dependence of the results with the number of *k*-points in the Brillouin zone taken into account. In our three-Ti-layer calculations, the reciprocal space was sampled using Monkhorst−Pack[22] special points sets 2 2 1. The norm-conserving pseudopotential optimizations were made using set 3 3 1. Only the three-Ti-layer structures with monolayer coverage were studied. The same optimization procedure was applied as in previous calculations.

The results for all systems are presented in the Table 1 and are similar to the results obtained using ultrasoft pseudopotentials with *k*-set 2 2 1. Table 1 shows that increasing the energy cutoff downshifts the energy of both the associative and dissociative adsorption but does not change their relative order.

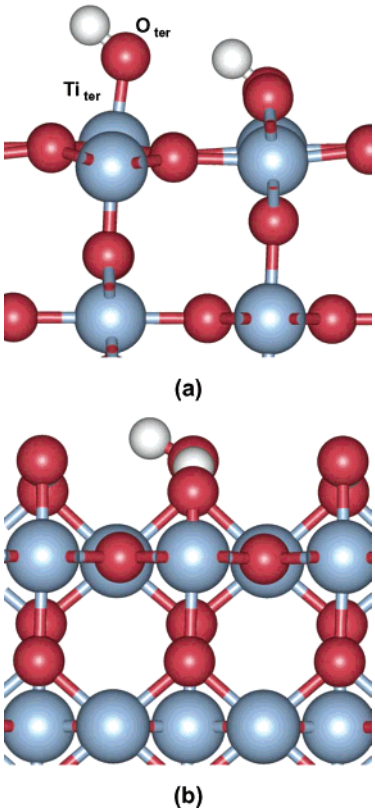

Figure 7. Dissociative adsorption, half-monolayer coverage: (a) structure 1, view in (001) direction; (b) structure 2, view in ($\bar{1}$10) direction.

Also, energy-minimized structures were not affected considerably when the 1000 eV energy cutoff and extended *k*-points set were used. The relative displacements of the surface atoms were almost the same for all three-Ti-layer slabs with identical water coverage (Table 2). In Table 1, the bond distances between the Ti atoms and the topmost O atoms using the different computational parameters are compared. The difference between the corresponding values does not exceed 0.05 Å for the chemical bonds within the crystal and 0.1 Å for the Ti−O_{H_2O} distances. The length of the Ti−O bonds lines up in the same order, Ti−O_{br} (bare surface) < Ti−O_{br} (associatively hydroxylated surface) < Ti−O_{ter} < Ti−O_{br} (dissociatively hydroxylated surface) < Ti−O_{H_2O}, for all calculated systems. Hence, we conclude that the results obtained using pseudopotentials and the 340 eV cutoff are reliable within the type of errors just mentioned.

4. LCAO 2-D Periodic Slab Calculations

In Table 4, the adsorption energies are listed for the periodic LCAO calculations. The HF method using both the all-electron and the ECP basis gives dissociative adsorption energies that are approximately 8 to 12 kJ/mol more favorable than those for associative adsorption. The DFT method results in the opposite picture: associative adsorption energies exceed the dissociative values by approximately 21 kJ/mol both for the three- and five-Ti-layer slabs. This fact may be attributed to the electron correlation effects which are taken into account by the Kohn−Sham Hamiltonian.

The basis set superposition error (BSSE) was estimated for the ECP three-Ti-layer hydroxylated slabs, and it appears to be 27 kJ/mol per one water molecule. The TiO_2 slabs with the dissociated and molecular form of H_2O have been calculated using exactly the same basis sets in all cases, so the large value of the BSSE influences the absolute values of ΔE only but not the relative energy of water dissociation on the TiO_2 surface. Taking into account the value of the BSSE, the absolute values of the obtained LCAO water adsorption energies seem to lie in the interval of 105−145 kJ/mol which is slightly greater than the corresponding CASTEP PW results.

The optimized structures of the bare TiO_2 surface and the hydroxylated (hydrated) slabs exhibit qualitatively the same relaxations as were found in the CASTEP PW calculations. But there are some quantitative differences between the results of the DFT-PW, DFT-LCAO, and HF-LCAO approximations. The *z*-shifts of the positions of the surface atoms on the TiO_2 slabs obtained by the LCAO methods are given in Table 5. Comparison of Tables 2 and 5 shows that the Kohn−Sham Hamiltonian (both on the PW and the LCAO basis) produces the larger expansion of the slabs toward the vacuum making them thicker and thus affects the vertical displacements of atoms to be more positive relative to the HF and experimental values. The same effect was found for hydroxylated and hydrated species: horizontal and vertical distortions of top surface O and Ti atoms from their bulk positions are substantially larger for DFT-LCAO than for HF-LCAO. Also, the DFT method leads to more flexible hydroxyl groups on hydroxylated surfaces and, as consequence, to shorter H-bonds between them.

The LCAO basis provides the possibility of calculating the atomic charges in a more direct way than the PW basis. In Tables 6 and 7, the charges on the surface atoms obtained via the Mulliken population analysis are listed. The values of the charges lie in a reasonable range and reflect the partially covalent nature of the chemical bonds in Ti oxides, although the HF method gives about 25% larger absolute values than the DFT

TABLE 4: Calculated (Without Zero-Point Correction) at Monolayer Coverage and Experimental Adsorption Energies (kJ/mol, Per One Water Molecule) for $H_2O/TiO_2(110)$[a]

method	molecular adsorption	dissociative adsorption	reference
PW:DFT-GGA-PW91, 340 eV; 3 Ti-L	−104	−96	this work
PW:DFT-GGA-PW91, 1000 eV; 3 Ti-L	−105	−103	this work
PW:DFT-GGA-PW91, 340 eV; 5 Ti-L	−92	−77	this work
PW:DFT-GGA-BP88, 1000 eV	−79	−104	Goniakowski et al. (1996)[1]
PW:DFT-GGA-PW91, 750 eV	−96	−88	Lindan et al. (1998)[5]
LCAO:HF, DB ECP; 3 Ti-L	−149	−156	this work
LCAO:HF, DB ECP; 3 Ti-L, with equal basis on all species (for BSSE)	−118	−121	this work
LCAO:HF, all-electron; 3 Ti-L	−118	−131	this work
LCAO:DFT-GGA-PW91, DB ECP; 3 Ti-L	−170	−152	this work
LCAO:DFT-GGA-PW91, DB ECP; 5 Ti-L	−147	−126	this work
experiment	−(59−100)		Brinkley et al. (1998)[11]

[a] *n* Ti-L designates the number of the Ti layer in the slab model.

TABLE 5: *z*-Shifts of Ti and O Atoms on the Bare Surface of (110) Rutile Three-Ti-Layer Models Obtained by LCAO Calculations

method:		HF, all-electron	HF, DB ECP	DFT, DB ECP	HF, all-electron[13]	exptl[30]
atom type	symbol	*z*-shifts, Å				
6-fold coordinated surface Ti	Ti_{6f}	0.13	0.15	0.19	0.09	0.12 ± 0.05
5-fold coordinated surface Ti	Ti_{5f}	−0.12	−0.12	−0.09	−0.15	-0.16 ± 0.05
bridging surface oxygen	O_{br}	−0.07	−0.07	0.01	−0.14	-0.27 ± 0.08
3-fold coordinated surface oxygens	O_{3f}	0.15	0.14	0.21	0.07	$0.05/0.16 \pm 0.08$
oxygen underneath O_{br}	O_{uO}	−0.02	−0.02	−0.01	−0.07	0.05 ± 0.08
oxygen underneath Ti_{5f} in the middle Ti layer	O_{uTi}	−0.01	0.01	0.03	−0.02	0.00 ± 0.08

TABLE 6: Atomic Charges (e^-) on the Surface of the (110) Rutile Three-Ti-Layer Models Obtained by HF-LCAO All-Electron Calculations

atom type	symbol	bare	associatively hydroxylated	dissociatively hydroxylated
titanium in the bulk TiO_2	Ti	2.438	2.432[a]	2.445[a]
6-fold coordinated surface Ti	Ti_{6f}	2.598	2.506	2.484
5-fold coordinated surface Ti, or 6-fold coordinated terminal Ti with OH group	Ti_{5f}, or Ti_{ter}	2.500	2.508	2.475
oxygen in the bulk TiO_2	O	−1.219	−1.214[a]	−1.222[a]
bridging surface oxygen	O_{br}	−1.228	−1.290	−1.035
3-fold coordinated surface oxygens	O_{3f}	−1.280	−1.242	−1.218
oxygen underneath O_{br}	O_{uO}	−1.289	−1.264	−1.193
oxygen underneath Ti_{5f} in the middle Ti layer	O_{uTi}	−1.238	−1.214	−1.249
terminal oxygen, or water oxygen	O_{ter}, or O_{H_2O}		−0.700	−0.951
hydrogen in terminal hydroxyl, or water hydrogen	H_{ter} or H_{H_2O}		0.352	0.324
hydrogen in bridging hydroxyl, or water hydrogen	H_{br} or H_{H_2O}		0.369	0.358

[a] Charges for atoms in the middle layer of the corresponding slab model.

TABLE 7: Atomic Charges (e^-) on the Surface of the (110) Rutile Three- and Five-Ti-Layer Models Obtained by DFT-LCAO Calculations Using Durand−Barthelat[25] ECP

		bare		associatively hydroxylated	dissociatively hydroxylated
atom type	symbol	3 Ti-L	5 Ti-L	5 Ti-L	5 Ti-L
titanium in the bulk TiO_2	Ti	1.858	1.844[a]	1.854[a]	1.861[a]
6-fold coordinated surface Ti	Ti_{6f}	1.755	1.758	1.734	1.807
5-fold coordinated surface Ti, or 6-fold coordinated terminal Ti with OH group	Ti_{5f}, or Ti_{ter}	1.824	1.813	1.793	1.802
oxygen in the bulk TiO_2	O	−0.929	−0.931[a]	−0.932[a]	−0.932[a]
bridging surface oxygen	O_{br}	−0.714	−0.694	−0.754	−0.760
3-fold coordinated surface oxygens	O_{3f}	−0.946	−0.969	−0.943	−0.933
oxygen underneath O_{br}	O_{uO}	−0.968	−0.932	−0.912	−0.900
oxygen underneath Ti_{5f} in the middle Ti layer	O_{uTi}	−0.926	−0.903	−0.923	−0.889
terminal oxygen, or water oxygen	O_{ter}, or O_{H_2O}			−0.581	−0.689
hydrogen in terminal hydroxyl, or water hydrogen	H_{ter} or H_{H_2O}			0.299	0.296
hydrogen in bridging hydroxyl, or water hydrogen	H_{br} or H_{H_2O}			0.312	0.320

[a] Charges for atoms in the middle layer of the corresponding slab model.

method. The deviations of atomic charges on the surface of the unhydroxylated slabs from their bulk values are generally less than 0.1 e^- both for the Ti and the O atoms, except the charge on the bridging oxygen obtained in the DFT calculations which is reduced by more than 0.2 e^-. The O atomic charges in the hydroxylated and hydrated slabs become less negative in the order $|q(O_{br})| > |q(O_{ter})| > |q(O_{H_2O})|$, which is correlated with the acidity of the corresponding hydroxyl groups on typical oxide surfaces.[34]

Our results demonstrate the relatively large dependence of the calculated water adsorption energies on the nature of the quantum mechanical approximation (HF or DFT) and the type of basis set within the same periodic slab model. It should be noted that the results for the equivalent 2-D and 3-D slab models coincide if a sufficiently large vacuum gap for the 3-D model is used.[17] Nevertheless, we can conclude that the Kohn−Sham Hamiltonian using both the PW and the LCAO basis sets gives an order of the adsorption energy which is in better agreement with the experimental observations.[8−11] However, the relaxation of the surface atoms seems to be more appropriate to the experimental data[30] in the case of the HF calculations.

5. Embedded Cluster Results

Our calculated adsorption energies are similar to those obtained by Stefanovich and Truong,[4] although a larger number of atoms were treated explicitly in this study. This result is useful because it can be used to justify limiting the size of the explicit cluster for computational efficiency. However, there is some dependence of the embedded cluster results on the cluster size, basis set, and method used. When the size of the cluster is increased, the energy difference between the associative and dissociative adsorption mechanisms decreases.

The results for the embedded cluster calculations were different from those for the periodic models. Adsorption energies of H_2O in the embedded cluster case were much more favorable for the associative mechanism (Table 8), which is in better agreement with the experimental observations.[8−10] The predicted

TABLE 8: Embedded Cluster Results (without BSSE) and Experimental Adsorption Energies for $H_2O/TiO_2(110)$ (kJ/mol)

method	cluster	molecular adsorption	dissociative adsorption	reference
LCAO:HF, LANL1-CEP	$Ti_{17}O_{34}$	−94[a]	−48[a]	this work
LCAO:HF, LANL2-CEP	$Ti_{13}O_{26}$	−158	−90	this work
LCAO:HF, LANL1-CEP	Ti_7O_{14}	−137[b]	−31[b]	Stefanovich et al. (1999)[4]
LCAO:B3LYP, LANL1-CEP	Ti_7O_{14}	−146	−95	Stefanovich et al. (1999)[4]
experiment		−(59−100)		Brinkley et al. (1998)[11]

[a] Estimated basis set superposition error is about 35 kJ/mol. [b] Estimated basis set superposition error is about 29 kJ/mol.

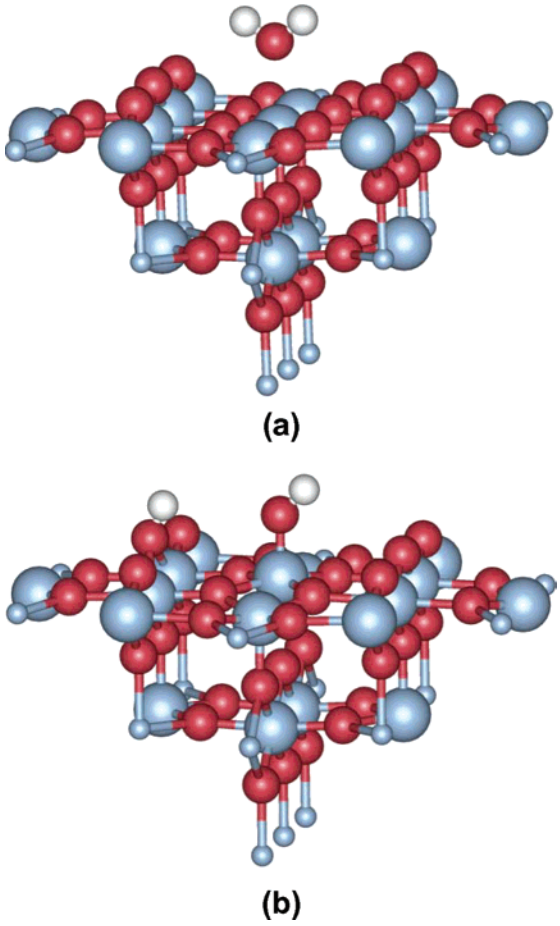

Figure 8. Embedded cluster results for the HF geometry of $Ti_{17}O_{34}-H_2O$: (a) associative adsorption; (b) dissociative adsorption. Small-sized balls represent the Ti pseudopotential cores.

adsorption energies for the associative mechanisms are larger than the measured values, however.[11] There is no considerable difference between the optimized geometry for water adsorption in $Ti_{13}O_{26}$ and $Ti_{17}O_{34}$: the structures of the latter are shown in Figure 8. No evidence of H-bond interactions was found in either the dissociative or associative adsorption structures in contrast to CASTEP and CRYSTAL calculations. Bridging oxygen atoms in the cluster model appear to exhibit less relaxation than in the periodic slabs. Whether this lack of H-bonding is the result of the lack of hydration of the other O atoms or whether this is an artifact of the method is a subject for future work.

The reason for such divergence between the two models (periodic and embedded cluster) is not entirely clear. The most probable reason is the difference in symmetry and boundary conditions: the absence of periodic boundary conditions in the embedded cluster model may lead to artificial rigidity of the TiO bonds. Also, the assignment of formal charges to lattice ions may overestimate the Madelung potential of the bulk crystal. On the other hand, the three- and five-layer periodic models apparently overestimate the surface relaxation and the thicker slabs are needed for improved quantities.

6. Conclusions

Our results correspond well with the experimental observation that the probability of H_2O dissociation is increased with decreasing surface coverage. One explanation of this change in mechanism with coverage is that H_2O molecules can readily align to provide the maximum H-bonding interaction in associatively adsorbed structures. At low coverages, H-bonding energies are not as significant as at higher coverages, so the additional energy of forming stronger Ti−OH bonds (as compared to $Ti-OH_2$ bonds) outweighs the H-bonding term, and dissociation may dominate.

Applying the different ab initio quantum mechanical approximations (DFT-PW, DFT-LCAO, or HF-LCAO) within the periodic models produces qualitatively close results, but disagreement may exist in reproducing the difference between close values if this difference is about several kJ/mol. In particular, the DFT-LCAO method gives an order of the associative and dissociative water adsorption energy which is in better agreement with the experimental observations.

Additional investigations of H-bonding between water molecules and oxygen atoms on the TiO_2 surface using both the DFT and HF methods should be made to resolve the disagreement between the periodic and embedded cluster calculations.

Acknowledgment. This research was supported by the U.S. Department of Energy, Office of Basic Energy Sciences, Division of Chemical Sciences, Geosciences and Biosciences, under the project "Nanoscale Complexity at the Oxide−Water Interface" and by NSF Grant EAR-0073722 "Adsorption of Cations on Mineral−Aqueous Solution Interfaces at Elevated Temperatures". We thank the anonymous reviewer who had several useful insights that improved this research. We are also grateful to Dr. Jorge Sofo (PSU) who has consulted with us on this project.

References and Notes

(1) Goniakowski, J.; Gillan, M. J. *Surf. Sci.* **1996**, *350*, 145−158.
(2) Vogtenhuber D.; Podloucky R.; Redinger, J. *Surf. Sci.* **1998**, *404*, 798−801.
(3) Casarin, M.; Maccato, C.; Vittadini, A. *J. Phys. Chem. B* **1998**, *102*, 10745−10752.
(4) Stefanovich, E. V.; Truong, T. N. *Chem. Phys. Lett.* **1999**, *299* (6), 623−629.
(5) (a) Lindan, P. J. D.; Harrison, N. M.; Holender, J. M.; Gillan, M. J. *Chem. Phys. Lett.* **1996**, *261*, 246−252. (b) Lindan, P. J. D.; Harrison, N. M.; Gillan, M. J. *Phys. Rev. Lett.* **1998**, *80*, 762−765.
(6) Zhang, C.; Lindan, P. J. D. *J. Chem. Phys.* **2003**, *118*, 4620−4630.
(7) Langel, W. *Surf. Sci.* **2002**, *496*, 141−150.
(8) Henderson, M. A. *Surf. Sci.* **1996**, *355*, 151−166.
(9) Henderson, M. A. *Langmuir* **1996**, *12*, 5093−5098.
(10) Hugenschmidt, M. B.; Gamble, L.; Campbell, C. T. *Surf. Sci.* **1994**, *302*, 329−340.
(11) Brinkley, T.; Dietrich, M.; Engel, T.; Farrall, P.; Gantner, G.; Schafer, A.; Szuchmacher, A. *Surf. Sci.* **1998**, *395*, 292−306.

(12) Stefanovich, E. V.; Truong, T. N. *J. Chem. Phys.* **1997**, *106*, 7700−7705; Stefanovich, E. V.; Truong, T. N. *J. Phys. Chem. B* **1998**, *102*, 3018−3022.
(13) Reinhardt, P.; Hess, B. A. *Phys. Rev. B* **1994**, *50*, 12015−12024.
(14) *Quantum-Mechanical Ab Initio Calculation of the Properties of Crystalline Materials*; Pisani, C., Ed.; Lecture Notes in Chemistry 67; Springer-Verlag: Berlin, 1996.
(15) Harrison, N. M.; Wang, X. G.; Muskat, J.; Scheffer, M. *Faraday Discuss.* **1999**, *114*, 305−312.
(16) Leconte, J.; Markovits, A.; Skalli, M. K.; Minot, C.; Belmajdoub, A. *Surf. Sci.* **2002**, *497*, 194−204.
(17) Evarestov, R. A.; Bandura, A. V. *Int. J. Quantum Chem.* **2004**, *96*, 282−291.
(18) (a) Bandura, A. V.; Sykes, D. G.; Kubicki, J. D. Derivation of Force Field Parameters for TiO_2−H_2O Systems from Ab Initio Calculations. *Abstracts of Papers*, National Meeting of the American Chemical Society, Orlando, FL, April, 2002; American Chemical Society: Washington, DC; 074-GEOC. (b) Bandura, A. V.; Kubicki, J. D. *J. Phys. Chem. B* **2003**, *107*, 11072−11081.
(19) Perdew, J. P. Unified Theory of Exchange and Correlation beyond the Local Density Approximation. In *Electronic Structure of Solids '91*; Ziesche, P. Eschrig, H., Eds.;. Akademic Verlag: Berlin, 1991; pp 110−2.
(20) *CASTEP—Cambridge Serial Total Energy Package User's Guide*, version 4.2; Molecular Simulations: San Diego, CA, 1999.
(21) Vanderbilt, D. *Phys. Rev. B* **1990**, *41*, 7892−7895.
(22) Monkhorst, H. J.; Pack, J. D. *Phys. Rev.* **1976**, *13*, 5188−5192.
(23) Perdew, J. P.; Burke, K.; Ernzerhof, M. *Phys. Rev. Lett.* **1996**, *77*, 3865−3868.
(24) Saunders, V. R.; Dovesi, R.; Roetti, C.; Orlando, R.; Zicovich-Wilson, C. M.; Harrison1, N. M.; Doll, K.; Civalleri, B.; Bush, I. J.; D'Arco, Ph.; Llunell, M. *CRYSTAL2003: User's Manual*; University of Turin: Torino, Italy, 2003.
(25) Durand, P.; Barthelat, J. C. *Theor. Chim. Acta* **1975**, *38*, 283−302.
(26) Fahmi, A.; Minot, C.; Silvi, B.; Causa, M. *Phys. Rev. B* **1993**, *47*, 11717−11724.
(27) Catti, M.; Sandrone, G.; Dovesi, R. *Phys. Rev. B* **1997**, *55*, 16122−16131.
(28) Hehre, W. J.; Ditchfield, R.; Pople, J. A. *J. Chem. Phys.* **1972**, *56*, 2257−2261.
(29) Frisch, M. J. et al. *Gaussian 98*, revision A.7; Gaussian, Inc.: Pittsburgh, PA, 1998.
(30) Charlton, G.; Howes, P. B.; Nicklin, C. L.; Steadman, P.; Taylor, J. S. G.; Muryn, C. A.; Harte, S. P.; Mercer, J.; McGrath, R.; Norman, D.; Turner, T. S.; Thornton, G. *Phys. Rev. Lett.* **1997**, *78*, 495−498.
(31) Hay, P. J.; Wadt, W. R. *J. Chem. Phys.* **1985**, *82*, 270−283.
(32) Stevens, W.; Basch, H.; Krauss, M. *J. Chem. Phys.* **1984**, *81*, 6026−6033.
(33) Stefanovich, E. V.; Shluger, A. L. *J. Phys.: Condens. Matter* **1994**, *6*, 4255−4268.
(34) Hiemstra, T.; Yong, H.; Van Riemsdijk, W. H. *Langmuir* **1999**, *15*, 5942−5955.